Controlled Release Characteristics of Aqueous PEO-PPO-PEO Micelles with added Malachite Green, Erythrosin, and Cisplatin determined by UV-Visible Spectroscopy

Andre Lamont Thompson;[a] Ashley N Ball;[a] Brian James Love[a,b,*]

[a]Department of Materials Science and Engineering, University of Michigan, Ann Arbor, MI, USA 48109

[b]Department of Biomedical Engineering, University of Michigan, Ann Arbor, MI, USA 48109

*Corresponding Author: bjlove@umich.edu

Abstract

Dynamic diffusion experiments were performed on aqueous polymeric micelles mixed with malachite green (0.05% mass v^{-1}), erythrosin (0.1% mass v^{-1}), and cisplatin (0.1% mass v^{-1}) to gauge release from sequestered structures using Ultraviolet-Visible spectroscopy. The additives were formulated with 20% mass v^{-1} aqueous solutions of polyethylene oxide-polypropylene oxide-polyethylene oxide, PEO-PPO-PEO (F127). Each additive was tested neat at room temperature, neat at 40°C, and formulated with F127 at room temperature, and 40°C. After constructing calibration curves, the dynamic release for each ternary additive and corresponding diffusion coefficients were calculated. Results show that F127 retards permeation at room temperature. In general, the neat additives at 40°C showed the highest permeability for both malachite green and erythrosin. Malachite green released almost 90% of the dye by 60 minutes of permeation. When formulated with F127 at 40°C, sizeable release was still noted, but with an induction period of 10-30 minutes to register release. The behavior with cisplatin was more complicated as the first 5 hours of permeation resulted in a burst delivery with cisplatin (6% total release with cisplatin-F127-RT compared to 4% total release cisplatin-RT) but with overall lower release. The higher fluence at elevated temperature is attributed to reducing the blocking effect of the amphiphiles on the walls of the dialysis tubing as they are directed to form colloidal gels.

This is the author manuscript accepted for publication and has undergone full peer review but has not been through the copyediting, typesetting, pagination and proofreading process, which may lead to differences between this version and the Version of Record. Please cite this article as doi: 10.1002/jsde.12001

There is also likely a correlation between higher temperature and higher overall permeability if the membrane pores also expand with temperature.

Keywords: surfactant, cisplatin, diffusion, drug delivery, malachite green chloride, erythrosin B dye

Introduction

One of the main treatments for both localized and metastatic cancer is chemotherapy, which is used in conjunction with surgery and radiotherapy [1]. It is ideal to deliver a sufficient quantity of drug to tumorous cells, while minimizing systemic side effects and toxicity. However, the drug effectiveness is retarded due to the complications with administering them such as inefficient distribution, limited chemotherapeutic solubility, an inability to permeate cell membranes, rapid clearance, and the lack of selectivity between normal cells and cancer cells [1]. Cis-dichlorodiammineplatinum(II) (cisplatin) is one of the most potent and widely-used anticancer drugs for treating testicular, ovarian, bladder, cervical, head, neck, oesophageal, and small-cell lung cancers [2, 3]. Cisplatin interacts with DNA and interferes with the normal cell transcription and replication processes, resulting in apoptosis [2, 4]. Despite its effectiveness, the clinical use of cisplatin and its derivatives is limited due to severe systemic side effects including nephrotoxicity, neurotoxicity, ototoxicity, nausea, and vomiting [5]. Therefore, developing efficient drug delivery systems that selectively increase the concentration of chemotherapeutics in diseased cells and tumors are of great significance and value.

To increase the therapeutic efficacy, chemotherapeutic drugs are often coupled with polymeric micelles and surfactants [6-8]. Blocky amphiphilic copolymers with a large solubility difference between hydrophilic and hydrophobic segments are known to assemble in an aqueous environment into polymeric micelles with a 10-100 nm size range [9-12]. These micelles have a narrow size distribution and are characterized by their core-shell architecture, where hydrophobic segments are segregated from the aqueous exterior to form a hydrophobic inner core surrounded

by hydrophilic segments [6]. Interests in applying block copolymer micelles as drug delivery systems have increased because of the high drug-loading capacity of the inner core as well as some level of increased tolerance of the drug loaded micelles compared to neat drugs [13-17].

The aggregation and surface properties of polymeric micelles in solution depend on external factors such as pH, temperature, pressure, and the presence of additives [18]. Thus, the properties of polymeric micelles in solution can be effectively tuned to a desired range and application by altering these external factors. Mandal et al has conducted various physicochemical studies on mixtures of PEO-PPO-PEO micelles and sodium dodecyl sulfate (SDS) in the absence and presence of various solubilized drugs, peptides, and additives as a function of various mole compositions using various techniques [19-21]. Moulik et al have also recently reported about the effect of various additives on aqueous normal and reverse PEO/PPO micelles [22]. Therefore, even though there are a variety of structures including microspheres [23, 24], dendrimers [25], liposomes [26-29], carbon nanohorns [30-32], carbon nanotubes [1], and nanoparticles; gold [33], silver [34], Fe_3O_4 [35, 36], pH-responsive [37, 38] and silica [39, 40]; that can be used as drug delivery agents, polymeric micelles' high drug-loading ability and toxicity shield effect [13-17] suggests they are sufficient drug delivery platforms to compliment other used drug delivery materials.

Our group has previously studied the effects a third component has on the driving force to form polyethylene oxide-polypropylene oxide-polyethylene oxide, PEO-PPO-PEO, micelles linked with thermodynamics [41, 42], structural evolution [43], and its gelation [44]. We have observed that the third species helps as a chaperone to coerce the formation of micelles and colloidal crystals, at lower temperature than what forms normally in the neat stage [41-44]. It is clear that the driving force to form a gel is influenced by the third component and as phase separation arises, the amphiphilic qualities of the additive likely have an effect on where within the forming micelles the ternary constituent is found [41, 42]. The location of the drugs within the micelle can also affect the permeability and bioavailability of drug elements sequestered within a forming colloidal gel [41, 42].

Our goal is to package cold chemotherapeutic drugs in these dispersions below their critical micelle temperatures, and inject them via syringe intratumoral, therefore bypassing an IV drip. Latent body temperature equilibration will trigger the micelle and gelation of the copolymer and drug within, causing the drug to be sequestered and alter the release characteristics over time rather than from solution. Here, we ran a series of diffusion experiments using dialysis tubing cellulose membrane on aqueous polymeric micelles (Pluronic® F127) mixed with ternary additives at two temperatures over time to study the release characteristics of micelles using Ultraviolet-Visible spectroscopy (UV-Vis) to monitor the release rate. The ternary additives studied here are cisplatin, malachite green chloride (green dye), and erythrosin B (red dye).

Experimental

Materials

Polyethylene oxide-polypropylene oxide-polyethylene oxide, PEO-PPO-PEO, Pluronic® F127 (12,600 g/mol molecular mass), malachite green chloride ($C_{23}H_{25}ClN_2$, 364.91 g/mol molecular mass), erythrosin B dye ($C_{20}H_8I_4O_5$, 835.89 g/mol molecular weight) and cisplatin ($[Pt(NH_3)_2Cl_2]$, 300.05 g/mol molecular mass) were all obtained from Sigma-Aldrich (Milwaukee, WI) and were used as received. The structures of each are shown in Figure 1. The dialysis tubing cellulose membrane, also obtained from Sigma-Aldrich (21 mm average diameter, 33 mm average flat width, 110 ml/ft capacity, 14,000 g/mol molecular mass cut-off), was soaked in deionized water at room temperature for 5 minutes prior to use.

Kinetics of release

Approximately 15 cm of cellulose membrane dialysis tubing was measured and placed into 500 ml of deionized water at room temperature for several minutes until the tube opened. Then, one end of the tube was sealed with a rubber band, while the other end remained open to receive the solution. 20 ml of each solution was added to each tube by pipette, and then the other end of the

tube was sealed with a rubber band (leaving space for a small air bubble between the liquid and the tied knot). The outside of the tube was rinsed with deionized water. The tube and a magnetic stirrer were placed into a 1000 ml beaker of 500 ml of water (either at room temperature or at 40C) on a hot plate. Aliquots of the receiving solution inside the beaker were measured at various times using UV-Vis to track the release rate for each ternary additive. A schematic of this setup is provided in Figure 2 [45].

Neat solutions of malachite green (10mg), erythrosin (20mg), and cisplatin (20mg) were each mixed into 20 ml room temperature water then aliquoted into the dialysis tubing. Aqueous solutions of F127 (4g) were each prepared according to the "cold" processing methods of Schmolka [46]. The ternary additives were then mixed into each solution containing F127 and aliquoted into the dialysis tubing. Total volume of deionized water was maintained by adding the same volume of fresh deionized water. Each cumulative release profile (in the form of increasing UV intensity vs time) of the ternary additives was calculated from the absorption vs concentration plots (calibration curves) for each neat ternary additive. Our cisplatin release values are compared to Cheng et al whom used porous hollow Fe_3O_4 nanoparticles for controlled release of cisplatin [35]. Their cumulative release profile of cisplatin was obtained via the concentration correction (the amount of cisplatin in each aliquot calculated to correct the overall cumulative releasing of cisplatin) of released cisplatin based on the following equation [35]:

$$C_t' = C_t + \frac{v}{V}\sum_0^{t-1} C_t \qquad (1)$$

where C_t' is the corrected concentration at time t, C_t is the apparent concentration at time t, v is the volume of the aliquots taken and V is the total volume of the solution. In this study, four separate conditions were tested for each ternary additive: neat additive at room temperature (20-25°C), neat additive at ~40°C (approx. body temperature), F127 mixed additive at room

temperature (20-25°C), and F127 mixed additive at ~40°C (approx. body temperature). Since each ternary additive has a different diffusion release rate, UV-Vis measurements were taken between 200 nm and 850 nm at varying times per each condition for more accurate calculations, using a Varian Cary 50 Bio UV-Visible Spectrophotometer (University of Michigan Van Vlack labs). All UV-Vis measurements for malachite green were analyzed every 10 minutes up to 1 hour for each condition. All UV-Vis measurements with erythrosin were analyzed every 30 minutes up to 3 hours for each condition. UV-Vis measurements involving cisplatin were analyzed for several hours throughout several days for each condition.

Results and Discussion:

Calibration Curves of Ternary Additives

To study the release kinetics of the encapsulated ternary additives in F127, we dialyzed solutions of malachite green, erythrosin and cisplatin in 500 ml deionized water at room temperature and 40°C and compared those results to dialysis of dispersions containing the same small molecules with F127 in 500 ml deionized water at room temperature and 40°C. The amount of ternary additive released from the micelle gels was measured by UV-Vis. Calibration curves for all three of the neat ternary additives: malachite green, erythrosin, and cisplatin, were calculated. Here, we show an example graphically the calibration curve of neat malachite green in Figure 3. In Table 1, we show a summary of our values of each ternary additives' wavelength ranges, concentration ranges (mg/ml), slopes, y-intercepts, and correlation values (R^2), and compare our results to the cisplatin complex by Basotra et al [47].

As shown in Figure 3, as the concentration of malachite green increases, the solution progressed from light green to a darker green tint that absorbed in 610-620 nm range. This linear relationship was true for erythrosin and cisplatin as well at other wavelengths. For erythrosin, as the concentration increases, the solution progressed from light pink to a darker pink tint that

absorbed in 520-530 nm range. Basotra et al mixed o-Phenylenediamine with cisplatin to form a green colored complex with wavelength ranges 700-710 nm [47]. For neat cisplatin, since the dissociation of the yellow solid colored cisplatin is a clear liquid, direct visual observation is not possible hence the importance of UV-Vis to measure absorbance in the UV (270-300 nm range).

The dynamic rise in absorption in the receiver solution was used to calculate the concentration of the diffused molecules in solution at a given time. During dialysis, aliquots of the solution were measured by UV-Vis to resolve a receiving solution concentration. The cumulative release of neat ternary additives and ternary additve-F127 at room temperatures and 40°C is shown in Figures 4, 5, and 6.

For cisplatin, unexpectedly during our experimentation, observable dark black particles formed both inside the dialysis tubing and outside the tubing floating around in the receiver solution. This indicates a reaction is occurring and forming dark colored precipitates that eventually settled at the bottom of the beaker. Both the neat cisplatin trials and the cisplatin-F127 experiments resulted in precipitation occurring faster and more obviously in the dispersion than in the neat solution. These observations suggest cisplatin is unstable in solution. The instability is more pronounced at elevated temperatures and encapsulating cisplatin in a polymeric micelle might be ineffective in somehow stabilizing cisplatin from its transformation potential. We previously opened an old, stored sample of unused cisplatin and noticed similar discoloration. Upon reviewing the literature, Cubells et al [48] concluded cisplatin is unstable in aqueous solutions and the primary mode of decomposition involves displacement of the chloride ligand so increasing the chloride ion concentration would likely improve the stability of the drug in aqueous solution [48-51]. We performed a calibration curve for the dark colored cisplatin and the results are in Table 1. Interestingly, the absorbance was much higher at the same concentrations for the dark colored cisplatin compared to the normal yellow colored cisplatin at slightly different wavelength ranges (250-270 dark colored compared to 270-300 neat cisplatin) which is indicated in Table 1 by their different slopes (0.3 neat cisplatin compared to 17.1 dark colored

cisplatin). Since the dark colored particles were observed throughout the experiment for every condition, the calibration curve for dark colored cisplatin was used in Figure 6 instead of the calibration curve results for neat cisplatin to calculate the concentration of diffused cisplatin in solution at a given time.

The kinetics of Malachite Green release

To study the release kinetics of the encapsulated malachite green in F127, we dialyzed neat malachite green in deionized water at room temperature and 40°C and compared those results to the dialyzed malachite green-F127 in deionized water at room temperature and 40°C. The amount of malachite green released from the micelle gels was measured by UV-Vis at wavelengths 610-620 nm shown in Figure 4.

Probably what is most valuable from this type of analysis is the ability to extract a mass diffusion coefficient measurement for each condition, the determinations of which is shown in Table 2. The thickness of the membrane and the surface area of the dialysis tube are needed to perform the calculation. Clearly mass transfer is easiest (highest diffusion coefficient) for the MG-40^{o}C without the amphiphile. Adding the amphiphile, MG-F127-40^{o}C, cuts the flux in half but as time went on later in this experiment, there was a noted rise in the permeation rate. Similar release characteristics were observed in the neat MG-RT sample. The most sluggish diffusion occurred when the amphiphiles were added and diffusion commenced at room temperature. One observable was that none of these experiments achieved a saturation dose over the time scale evaluated. Clearly, the driving force for continued permeation existed for all experiments and we cannot comment on whether there was a difference in total release.

The rationale for why elevated temperature led to higher permeation is clear. There is higher Brownian motion in the solution when the temperature is raised from room temperature to 40^{o}C, and it is possible that the pore dimensions grow making the membrane more permeable with higher temperature as well. The increased activity of the higher temperature solution

explains why the neat solutions show higher flux and a higher apparent diffusion coefficient at higher temperature.

The presence of the amphiphile has two likely physical outcomes. At elevated temperature, there is clearly enough energy to trigger the formation of the colloidal crystals and the more the amphiphiles are organized into bulk structures in solution, the lower the probability that the surfactants are bound to the wall of the membrane blocking MG transport. If the amphiphiles organize into hydrophobic cores, those regions are effectively excluded volume for aqueous soluble MG which will raise the concentration in the water phase and increase the mass flux across the boundary. Of course, if MG was strongly bound to regions of the amphiphiles because micelles have larger micellar hydrodynamic radii at elevated temperatures, there might be a lower driving force for allowing MG to permeate out of the dispersion. Clearly, lower transport was not observed.

Lower temperature lowers the driving force for forming micelles and gels. Our group has pointed out that the typical micelle formation temperatures dropped with higher concentrations of F127 and with some ternary additives that interact with the micelle regulating the energetics of micelle formation [41-44]. If the driving force to form micelles is small, it is quite possible that more adsorbed surfactant is blocking pores in the membrane. Clearly, the lower temperature is also reducing the Brownian motion as well, but comparing MG-RT and MG-F127-RT, the presence of the surfactant is a strong impediment to permeation. Considering F127 reduced the release rate of malachite green at room temperature and 40^{o}C, this suggests it would offer a desired platform for drug delivery and release.

The kinetics of Erythrosin release

To study the release kinetics of the encapsulated erythrosin in F127, we dialyzed neat erythrosin in deionized water at room temperature and 40°C and compared those results to the dialyzed erythrosin-F127 in deionized water at room temperature and 40°C. The amount of erythrosin

released from the micelle gels was measured by UV-Vis at wavelengths 520-530 nm shown in Figure 5.

The diffusion coefficient measurements for each erythrosin condition is provided in Table 2. Similar to malachite green, the highest flux for erythrosin is ER-40^{o}C without the amphiphile. Adding the amphiphile, ER-F127-40^{o}C, cut the flux in half but as time went on in the experiment, there was a noted burst in the permeation rate. There was no observable change in release characteristics between the neat ER-RT and ER-F127-RT samples as both showed very low release (below 10%).

Similar to malachite green, none of these experiments achieved a saturation dose over the time scale evaluated. The driving force for continued permeation existed for all experiments, but we cannot comment on whether there was a difference in total release. At 40^{o}C, once again the Brownian motion is higher and that explains why the diffusion coefficient for ER-40^{o}C is the highest in the neat conditions for the first 150 minutes.

The presence of the amphiphile at elevated temperature cut the mass transfer rate in half for the first 150 minutes. There was enough energy to form colloidal crystals lowering the probability that the surfactants were bound to the wall of the membrane blocking the ER transport. If ER was strongly bound to regions of the amphiphiles, there might be a lower driving force for allowing ER to permeate out of the dispersion. This was not observed as a diffusion coefficient of 1.0 ± 0.01 x 10^{-6} cm^2sec^{-1} was found under this condition. After 150 minutes, we observed an increasing release of ER that was not observed with MG making the overall dynamic release curve more non-linear. The molecular mass of ER is larger than that of MG, so it takes longer for ER molecules to percolate through the gel and the membrane. This is an indication that while F127 does have a diffusion rate limiting effect on ternary additives, the rate at which the diffusion is limited varies for each ternary additive due to the molecular mass of the ternary additives. According to Mandal [52], translational and rotational motion diffusion coefficients can occur in solution simultaneously either in series or parallel. In congested

polymeric micellar conditions, there is a possibility of self-diffusion (slow process) and mutual or collective diffusion (fast process). These conditions are indistinguishable when the small amount of supporting electrolytes and buffer solutions are present in the systems [53-57]. With the method used here, a diffusion coefficient can be determined, but the non-linearity of the ER release suggests its non-Fickian and a different model is more appropriate.

Lowering the temperature lowers the driving force for forming micelles and gels. If the driving force to form micelles is small, it is possible that more adsorbed surfactant is blocking the pores in the membrane. The lower temperature also reduces the Brownian motion. In this case, for ER-RT and ER-F127-RT, the driving force for diffusing ER is so low at room temperature, that similar results were observed with and without the amphiphile. Considering F127 still reduced the release rate of ER in both conditions, this is another indication that suggests it would offer a desired platform for drug delivery and release.

Conceptually, erythrosin permeation through the dialysis membranes has a similar profile to MG. The hydrophilic erythrosin is concentrated in the aqueous regions and excluded from the hydrophobic cores of the micelles which increases the concentration gradient across the dialysis membrane once micelles form. And at elevated temperature, the pores in the membrane are larger.

The kinetics of cisplatin release

The same protocol was used for dialyzed neat cisplatin in deionized water at room temperature and 40°C and compared to that of dialyzed cisplatin-F127 in deionized water at room temperature and 40°C. The amount of cisplatin released from the micelle gels was measured by UV-Vis at wavelengths 250-270 nm shown in Figure 6. The cumulative release results in general compares well to previous cisplatin encapsulated drug delivery systems [35, 1, 58-60]. Guven et al reported less than 25% total released cisplatin from their Pluronic® F108-wrapped, W-CDDP@US-tubes after 200 hours [1]. Cheng et al reported less than 10% total cisplatin release

from their Fe-cisplatin loaded nanoparticles, Pt-PHNPs, at pH 7.4, 6, and 5 after 70 hours [35]. Reardon et al reported less than 20% cumulative release of cisplatin after 10 hours from their core-shell poly(lactic-co-glycolic acid) (PLGA) nanoparticles [58]. Fang et al reported less than 25% total cisplatin release from their chitosan hydrogels after 5 hours [59]. Czarnobaj and Lukasiak [60] reported less than 50% cisplatin release after 20 hours from their silica (SiO_2) xerogels at room temperature and 120^{o}C.

The diffusion results were unlike a normal diffusion profile. We observe a burst condition for three of the solution conditions including cisplatin neat (cisplatin-RT) in water at 25^{o}C, and for both dispersions (cisplatin-F127-RT and cisplatin-F127-40^{o}C)) at ambient temperature and at 40^{o}C. Reardon et al and Fang et al both also observed an initial burst release of cisplatin from their core-shell PLGA nanoparticles [58] and chitosan hydrogels [59]. It is worth noting that the size of the initial burst release is on the order of 8-9% while the neat MG and erythrosin release substantially more over the 150 hours of experimentation. We calculated a diffusion coefficient for the short, initial burst phase, but it is clear that three of the four conditions, there is burst followed by a much smaller release, compared with the systematic release of other dye molecules. The diffusion coefficient measurements for each cisplatin condition is provided in Table 2. From the analysis, the highest flux observed for cisplatin was cisplatin-F127-RT. The cisplatin-F127-RT release was slightly higher than cisplatin-RT.

There was no observable diffusion for neat cisplatin-40^{o}C in the first 5 hours. However, cisplatin was observed at much longer times finally permeating through after 50 hours. More Brownian motion should occur in the higher temperature neat systems but maybe there is a larger driving force to also transform and precipitate neat cisplatin as opposed to driving it across the dialysis membrane.

The presence of the amphiphile at elevated temperature increased the permeation for the first 5 hours relative to the neat system. This is possibly due to F127 interacting with cisplatin as we observed the formation of dark colored particles floating around in solution. If cisplatin was

strongly bound to hydrophilic or hydrophobic regions of the amphiphiles, there might be a lower driving force to allow cisplatin to permeate out of the dispersion. This was not observed as a diffusion coefficient of $1.2 \pm 0.1 \times 10^{-6}$ cm^2s^{-1} was found under this condition. Continued release past the burst period is observed and there are indications of a plateau concentration is evident at ~8% drug release at longer times. So a little less than half the release comes in the first 5 hours and the rest with longer exposure

Lowering the temperature lowers the driving force for forming micelles and gels. The lower temperature also reduces the Brownian motion. We observed a slightly higher initial burst at room temperature for the dispersion (F127-cisplatin RT) relative to the neat solution (cisplatin-RT). Since continued release of cisplatin occurred over time even after the initial burst, (3% release after 5 hours compared to 8% release after 144 hours), the presence of the amphiphile may aid in transporting cisplatin across a membrane.

Only with the dispersion at elevated temperature (cisplatin-F127-40^{o}C) is a plateau in permeation observed. There is a noted decrease in UV-Vis absorption for the other three conditions. Clearly with black particles forming while conducting the diffusion experiments, one rational for the lower absorption at later times might be due to the sedimentation of converted cisplatin particles that are not suspended in solution. If particles are denser than the fluid medium of the receiver solution, it is possible that the particles drift to the bottom of the receiver solution and are not sensed as part of the absorption at later time. If there was a nucleation and growth mechanism regulating particle formation, if the particles grew in size with time, they might be separated in the two-phase dispersion of particles in the receiver reservoir. We observed significant particle accumulation at the bottom of the reservoir as well. If the particle formation is linked with the inactivation of cisplatin, perhaps doing the experiments in saline solution might preserve the activity of the cisplatin and keep it in solution as opposed to directing its formation of a second particle phase as a dispersion.

Comparing the molecular structures of cisplatin with MG and ER, the two dyes are both stable and hydrophilic, while cisplatin is clearly unstable and perhaps more ambiguous in terms of its overall hydrophilicity. If the same mechanism of liberating the pores occurs with the amphiphile coalescence and formation of hydrophobic cores, if cisplatin was more drawn to the interface between the core and shell, that would reduce the amount available at the membrane boundary. With a time dependent stability issue, even if cisplatin was labile outside of the cores within the dialysis membrane, the fact that there is a nucleation and growth of the dark particulates which quickly grew larger than the pore dimensions of the membrane.

Comparison to other permeation experiments

Table 2 presents our results and includes a comparison of cisplatin diffusion coefficient values in a variety of delivery systems. The table includes references for cisplatin released from PLGA nanoparticles [58], PLGA microspheres, solid fibers, and hollow fibers [61], and chitosan-alginate nanoparticles [62].

Our diffusion results are higher than Campbell et al who observed much slower cisplatin diffusivity from PLGA microspheres [61]. Campbell's lower diffusivity of cisplatin was caused by the low molecular mobility of the matrices where cisplatin is encapsulated. Campbell et al reported some microspheres engulfed other microspheres with shell-like pores surrounding some regions of a microsphere causing droplets of oil phase to disperse in the aqueous phase. The low porosity of these microspheres suggests more sluggish drug permeability as there are few aqueous channels to allow paths for drug escape [61]. Campbell also observed a cumulative drug release over 500 hours, while our reported diffusion coefficient numbers are within the first 5 hours of release.

Our diffusion results are also higher than Campbell et al for diffused cisplatin from PLGA solid and hollow fibers [61]. Campbell reported during fiber drying, as more solvent is extracted during the phase inversion, the oil phase becomes a poorer solvent to the polymer

chains, and the chains retract and interact more with each other causing the glass transition temperature, Tg, to increase [61]. Since the polymer chains are less mobile, the diffusivity of the solvent in the oil phase decreases thus reduces the volume of the core, causing lower drug release [61]. Campbell also observed a cumulative drug release over 200 hours for solid fibers, and 400 hours for hollow fibers [61].

Our diffusion coefficients appear quite low, relative to Maan et al for in vitro release of cisplatin from electrostatically cross-linked chitosan-alginate nanoparticles [62]. This discrepancy could be due to the differences in our controlled drug release methods. Our polymeric micelles form gels at elevated temperatures, which encapsulates cisplatin, thus significantly reduces its permeation. Maan et al's release of the cisplatin complex from the nanoparticles involves the absorption of water into the nanoparticles matrix and simultaneous release of the drug via diffusion. When Maan's drug encapsulated nanoparticles are exposed to water, the polymer swells causing the T_g of the polymer to drop relative to the experimental temperature [62]. The release of the drug is regulated by the process of relaxation of macromolecular chains and the diffusion of the entrapped drug molecules into the exterior medium [62]. The Maan effort was tied to diffusion on a molecular level and our membrane dimensions are on the order of 100 microns, much larger overall. Man et al also observed a cumulative drug release within 2 hours, while our reported diffusion coefficient numbers are within the first 5 hours of release.

Our diffusion results are also very low compared to Reardon et al for cisplatin release from core-shell PLGA nanoparticles [58]. This discrepancy could be due to Reardon et al observed their cumulative release over 150 hours compared to our calculations after 5 hours. The Reardon effort also fabricated a drug delivery system on the Nano scale while our system is on the micro scale. Reardon et al also observed their diffusion study in Phosphate-buffered saline (PBS) while our study was observed in deionized water.

Conclusions

In summary, we demonstrated an approach using amphiphilic polymeric micelles (F127) to regulate controlled release of two indicator dyes (malachite green and erythrosin) and one chemotherapeutic drug (cisplatin). We tested the release at temperatures that would alter the driving force for forming colloidal gels in vivo (room temperature and 40^{o}C). We show the process tracking dye or drug collection in a receiver solution through a dialysis membrane from the absorbance measurements, via UV-Vis, to the determination of an apparent diffusion coefficient where applicable. Our cisplatin results were compared to a number of other studies in which permeation in a sequestered nanostructure was evaluated for its fluence [61, 62]. Adding the amphiphile lowered the permeability of dye molecules ($2.6 \pm 0.01 \times 10^{-7}$ cm^2s^{-1} MG-RT compared to $2.6 \pm 0.01 \times 10^{-8}$ cm^2s^{-1} MG-F127-RT), but tended to result in a burst delivery with cisplatin (6% total release with cisplatin-F127-RT compared to 4% total release cisplatin-RT). We noted instability with cisplatin in aqueous solution [48-51].

Acknowledgements

We acknowledge the Rackham Graduate School at UM for support. We would also like to thank the GEM Fellowship funded through DuPont and the National Physical Science Consortium (NPSC) fellowship funded through the National Institute of Standards and Technology (NIST) for their financial support. Thanks to Tim Chambers for training on the UV-Vis at UM Van Vlack Labs.

References

1. Guven A, Rusakova IA, Lewis MT, Wilson LJ. Cisplatin@US-tube carbon nanoparticles for enchanced chemotherapeutic delivery. Biomaterials. 2012;5(33):1455-61.
2. Cepeda V, Fuertes MA, Castilla J, Alonso C, Quevedo C, Perez JM. Biochemical mechanisms of cisplatin cytotoxicity. Anti-Cancer Agents in Medicinal Chemistry. 2007;7:3-18.
3. Lebwohl D, Canetta R. Clinical development of platinum complexes in cancer therapy: an historical perspective and an update. European Journal of Cancer. 1998;34(10):1522-34.
4. Siddik ZH. Cisplatin: mode of cytotoxic action and molecular basis of resistance. Oncogene. 2003;22:7265-79.
5. Wang D, Lippard SJ. Cellular processing of platinum anticancer drugs. Nature Reviews Drug Discovery. 2005;4:307-20.
6. Kataoka K, Harada A, Nagasaki Y. Block copolymer micelles for drug delivery: design, characterization and biological significance. Advanced Drug Delivery Reviews. 2001;47:113-31.
7. Nasongkla N, Bey E, Ren J, Ai H, Khemtong C, Guthi JS et al. Multifunctional polymeric micelles as cancer-targeted, MRI-Ultrasensitive drug delivery systems. Nano Letters. 2006;6(11):2427-30.
8. Nishiyama N, Okazaki S, Cabral H, Miyamoto M, Kato Y, Yuichi S et al. Novel cisplatin-incorporated polymeric micelles can eradicate solid tumors in mice. Cancer Research. 2003;63:8977-83.
9. Moffitt M, Khougaz K, Eisenberg A. Micellization of ionic block copolymers. Accounts of Chemical Research 1996;29:95-102.
10. Tuzar Z, Kratochvil P. Block and graft copolymer micelles in solution. Advances in Colloid and Interface Science. 1976;6:201-32.
11. Munk P, Prochazka K, Tuzar Z, Webber SE. Exploiting polymer micelle technology. CHEMTECH. 1998;28(10):20-8.

12. Talingting MR, Munk P, Webber SE. Onion-type micelles from polystyrene-block-poly(2-vinylpyridine) and poly(2-vinylpyridine)-block-poly(ethylene oxide). Macromolecules. 1999;32:1593-601.

13. Kwon GS, Kataoka K. Block copolymer micelles as long-circulating drug vehicles. Advanced Drug Delivery Reviews. 1995;16:295-309.

14. Kreuter J, Attwood D, Bouwstra JA, Crommelin DJA, Hofland HEJ, Junginer HE et al. Colloidal drug delivery systems. Drugs and the Pharmaceutical Sciences. New York: Marcel Dekker, Inc.; 1994.

15. Scholes PD, Coombes AGA, Davis MC, Illum L, Davis SS. Particle engineering of biodegradable colloids for site-specific drug delivery. Controlled Drug Delivery Challenges and Strategies, American Chemical Society. 1997:73-106.

16. Cammas S, Kataoka K. Site specific drug-carriers: polymeric micelles as high potential vehicles for biologically active molecules. Solvents and Self-Organizations of Polymers. NATO ASI Series E: Applied Sciences, Kluwer, Dordrecht; 1996.

17. Kwon GS, Okano T. Polymeric micelles as new drug carriers. Advanced Drug Delivery Reviews. 1996;21:107-16.

18. Verma SK, Ghosh KK. Micellar and surface properties of some monomeric surfactants and a gemini cationic surfactant. Journal of Surfactants and Detergents. 2011;14:347-52.

19. James J, Ramalechume C, Mandal AB. Two-dimentional surface properties of PEO-PPO-PEO triblock copolymer film at the air/water interface in the absence and presence of Tyr-Phe dipeptide, Val-Tyr-Val tripeptide, SDS and stearic acid. Colloids and Surfaces B: Biointerfaces. 2011;82:345-53.

20. James J, Mandal AB. Micelle formation of Tyr-Phe dipeptide and Val-Tyr-Val tripeptide in aqueous solution and their influence on the aggregation of SDS and PEO-PPO-PEO copolymer micelles. Colloids and Surfaces B: Biointerfaces. 2011;84:172-80.

21. Prameela GKS, Kumar BVNP, Aswal VK, Mandal AB. Influence of water-insoluble nonionic copolymer $E_6P_{39}E_6$ on the microstructure and self-aggregation dynamic of aqueous

SDS solution - NMR and SANS investigations. Physical Chemistry Chemical Physics. 2013;15:17577-86.
22. Naskar B, Ghosh S, Moulik SP. Solution behavior of normal and reverse triblock copolymers (Pluronic L44 and 10R5) individually and in binary mixture. Langmuir. 2012;28:7134-46.
23. Matsumoto A, Matsukawa Y, Suzuki T, Yoshino H, Kobayashi M. The polymeralloys method as a new preparation method of biodegradable microspheres: principle and application to cisplatin-loaded microspheres. Journal of Controlled Release. 1997;48:19-27.
24. Mathiowitz E, Jacob JS, Jong YS, Carino GP, Chickering DE, Chaturvedi P et al. Biologically erodable microspheres as potential oral drug delivery systems. Nature. 1997;386:410-4.
25. Gillies ER, Frechet JMJ. Dendrimers and dendritic polymers in drug delivery. Drug Discovery Today. 2005;10(1):35-43.
26. Samad A, Sultana Y, Aqil M. Liposomal drug delivery systems: an update review. Current Drug Delivery. 2007;4:297-305.
27. Yatvin MB, Weinstein JN, Dennis WH, Blumenthal R. Design of liposomes for enhanced local release of drugs by hyperthermia. American Association for the Advancement of Science. 1978;202(4374):1290-3.
28. Allen TM. Liposomal drug formulations: rational for development and what we can expect for the future. Drugs. 1998;56(5):747-56.
29. Ramachandran S, Quist AP, Kumar S, Lal R. Cisplatin nanoliposomes for cancer therapy: AFM and fluorescence imaging of cisplatin encapsulation, stability, cellular uptake, and toxicity. Langmuir. 2006;22:8156-62.
30. Ajima K, Yudasaka M, Murakami T, Maigne A, Shiba K, Iijima S. Carbon Nanohorns as anticancer drug carriers. Molecular Pharmaceutics. 2005;2(6):475-80.
31. Ajima K, Murakmi T, Mizoguchi Y, Tsuchida K, Ichihashi T, Iijima S et al. Enhancement of in vivo anticancer effects of cisplatin by incorporation inside single-wall carbon nanohorns. ACS Nano. 2008;2(10):2057-64.

32. Murakami T, Ajima K, Miyawaki J, Yudasaka M, Iijima S, Shiba K. Drug-loaded carbon nanohorns: adsorption and release of dexamethasone in vitro. Molecular Pharmaceutics. 2004;1(6):399-405.

33. Mohanty RK, Thennarasu S, Mandal AB. Resveratrol stabilized gold nanoparticles enable surface loading of doxorubicin and anticancer activity. Colloids and Surfaces B: Biointerfaces. 2014;114:138-43.

34. Mandal A, Sekar S, Chandrasekaran N, Mukherjee A, Sastry T. Poly(ethylene) glycol-capped silver and magnetic nanoparticles: synthesis, characterization, and comparison of bactericidal and cytotoxic effects. Journal of Engineering in Medicine. 2013;227(11):1224-36.

35. Cheng K, Peng S, Xu C, Sun S. Porous hollow Fe_3O_4 nanoparticles for target delivery and controlled release of cisplatin. Journal of the American Chemical Society. 2009;131(30):10637-44.

36. Mandal A, Sekar S, Kanagavel M, Chandrasekaran N, Mukherjee A, Sastry TP. Collagen based magnetic nanobiocomposite as MRI contrast agent and for targeted delivery in cancer therapy. Biochmica et Biophysica Acta. 2013;1830:4628-33.

37. Xu P, Kirk EAV, Murdoch WJ, Zhan Y, Isaak DD, Radosz M et al. Anticancer efficacies of cisplatin-releasing pH-responsive nanoparticles. Biomacromolecules. 2006;7:829-35.

38. Oishi M, Hayashi H, Iijima M, Nagasaki Y. Endosomal release and intracellular delivery of anticancer drugs using pH-sensitive PEGylated nanogels. Journal of Materials Chemistry. 2007;17:3720-5.

39. Barbe C, Bartlett J, Kong L, Finnie K, Lin HQ, Larkin M et al. Silica particles: a novel drug-delivery system. Advanced Materials. 2004;16(21):1959-66.

40. Slowing II, Trewyn BG, Giri S, Lin VS-Y. Mesoporous silica nanoparticles for drug delivery and biosensing applications. Advanced Functional Materials. 2007;17:1225-36.

41. Thompson AL, Love BJ. Thermodynamic properties of aqueous PEO-PPO-PEO micelles with added methylparaben determined by differential scanning calorimetry. Journal of Colloid And Interface Science. 2013;398(C):270-2. doi:10.1016/j.jcis.2013.01.064.

42. Thompson AL, Love BJ. Thermodynamic properties of aqueous PEO-PPO-PEO micelles of varying hydrophilicity with added cisplatin determined by differential scanning calorimetry. Journal of Thermal Analysis and Calorimetry. 2016;127(2):1583-92.
43. Meznarich NAK, Juggernauth KA, Batzli KM, Love BJ. Structural changes in PEO–PPO–PEO gels induced by methylparaben and dexamethasone observed using time-resolved SAXS. Macromolecules. 2011;44(19):7792-8. doi:10.1021/ma2015358.
44. Meznarich NAK, Love BJ. The kinetics of gel formation for PEO−PPO−PEO triblock copolymer solutions and the effects of added methylparaben. Macromolecules. 2011;44(9):3548-55. doi:10.1021/ma200302s.
45. Team SE. Selective permeability of dialysis tubing lab: explained. Creative Commons 4.0. 2010-2017. https://schoolworkhelper.net. 2017.
46. Schmolka IR. Artificial skin I. preparation and properties of pluronic F-127 gels for treatment of burns. Journal of Biomedical Materials Research. 1972;6:571-82.
47. Basotra M, Singh SK, Gulati M. Development and validation of a simple and sensitive spectrometric method for estimation of cisplatin hydrochloride in tablet dosage forms: application to dissolution studies. ISRN Analytical Chemistry. 2013;2013:1-8.
48. Cubells MP, Aixela JP, Brumos VG, Pou SD, Flaque MV. Stability of cisplatin in sodium chloride 0.9% intravenous solution related to the container's material. Pharmacy World & Science. 1993;15(1):34-6.
49. Banerjea D, Basolo F, Pearson RG. Mechanism of substitution reactions of complex ions. XII. Reactions of some platinum(II) complexes with various reactants. Reactions of Platinum Complexes with Various Reactants. 1957;79:4055-62.
50. Reishus JW, Don S. Martin J. cis-Dichlorodiammineplatinum(II). Acid hydrolysis and isotopic exchange of the chloride ligands. Acid Hydrolysis of cis-dichlorodiammineplatinum(II). 1961;83:2457-62.

51. Lee KW, D. S. Martin J. Cis-dichlorodiammineplatinum(II). Aquation equilibria and isotopic exchange of chloride ligans with free chloride and tetrachloroplatinate(II)*. Inorganica Chimica Acta. 1976;17:105-10.
52. Mandal AB. Shape, size, hydration and flow behavior of nitrocellulose lacquer emulsion in absence and presence of urea. Journal of the American Oil Chemists' Society. 1987;64(8):1202-7.
53. Mandal AB, Nair BU. Cyclic voltammetric technique for the determination of the critical micelle concentration of surfactants, self-diffusion coefficient of micelles, and partition coefficient of an electrochemical probe. Journal of Physical Chemistry. 1991;95:9008-13.
54. Mandal AB. Self-diffusion studies on various micelles using ferrocene as electrochemical probe. Langmuir. 1993;9:1932-3.
55. Geetha B, Mandal AB. Self-diffusion studies on É-methoxy polyethylene glycol macromonomer micelles by using cyclic voltammetric and fourier transform pulsed gradient spin-echo nuclear magnetic resonance techniques. Langmuir. 1995;11:1464-7.
56. Geetha B, Mandal AB. Determination of the critical micelle concentration of the methoxy polyethylene glycol based macromonomer and partition coefficient of a new electrochemical probe using a cyclic voltammetric technique. Langmuir. 1997;13:2410-3.
57. James J, Ramalechume C, Mandal AB. Self-diffusion studies on PEO-PPO-PEO triblock copolymer micelles in SDS micelles and vice versa using cyclic voltammetry. Chemical Physics Letters. 2005;405:84-9.
58. Reardon PJ, Parhizkar M, Harker AH, Browning RJ, Vassileva V, Stride E et al. Electrohydrodynamic fabrication of core-shell PLGA nanoparticles with controlled release of cisplatin for enhanced cancer treatment. International Journal of Nanomedicine. 2017;12:3913-26.
59. Fang J-Y, Chen J-P, Leu Y-L, Hu J-W. The delivery of platinum drugs from thermosensitive hydrogels containing different ratios of chitosan. Drug Delivery. 2008;15:235-43.

60. Czarnobaj K, Lukasiak J. In vitro release of cisplatin from sol-gel processed organically modified silica xerogels. Journal of Materials Science: Materials in Medicine. 2007;18:2041-4.
61. Campbell CS, Delgado-Charro MB, Camus O, Perera S. Comparison of drug release from PLGA microsperes and novel fibre formulations. Journal of Biomaterials Applications. 2016;30(8):1142-53.
62. Maan GK, Bajpai J, Bajpai AK. Investigation of in vitro release of cisplatin from electrostatically crosslinked chitosan-alginate nanoparticles. Synthesis and Reactivity in Inorganic, Metal-Organic, and Nano-Metal Chemistry. 2016;46:1532-40.

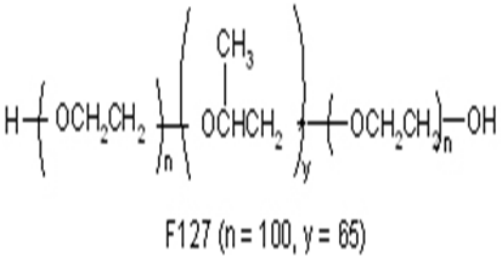

F127 (n = 100, y = 65)

(a)

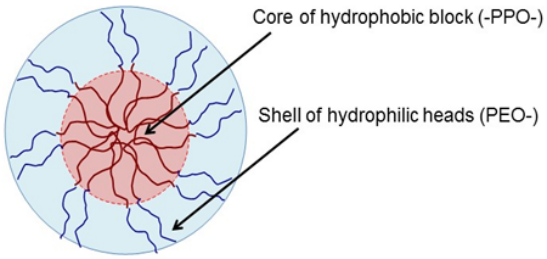

(b)

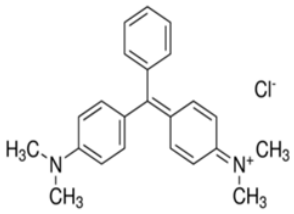

(c)

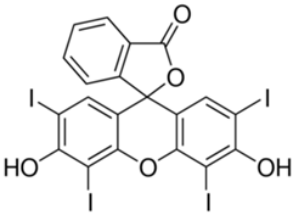

(d)

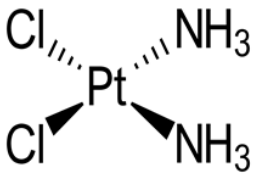

(e)

jsd-17-0248-File002.tif

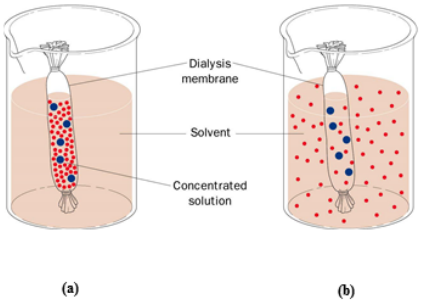

jsd-17-0248-File003.tif

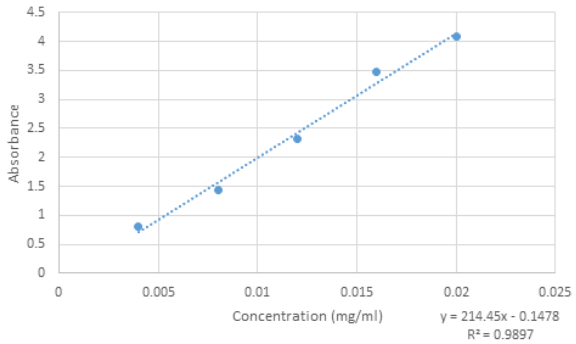

jsd-17-0248-File004.tif

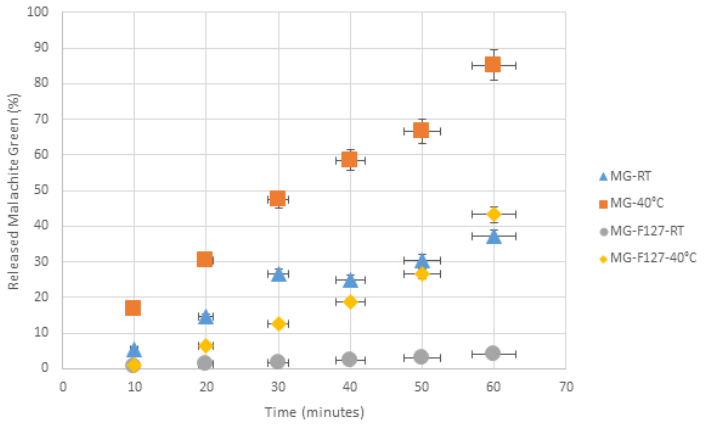

jsd-17-0248-File005.tif

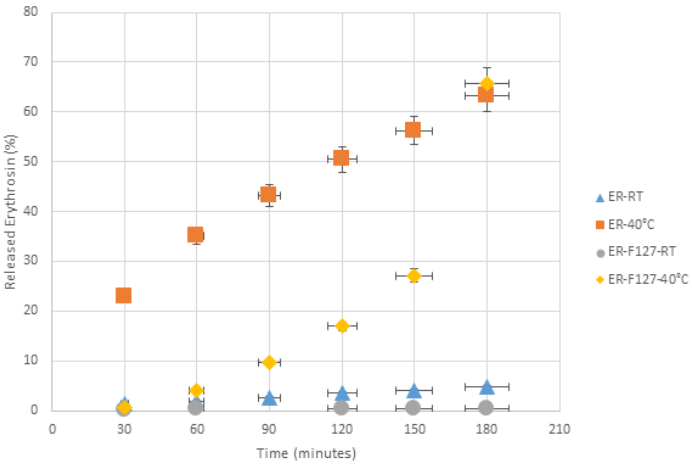

jsd-17-0248-File006.tif

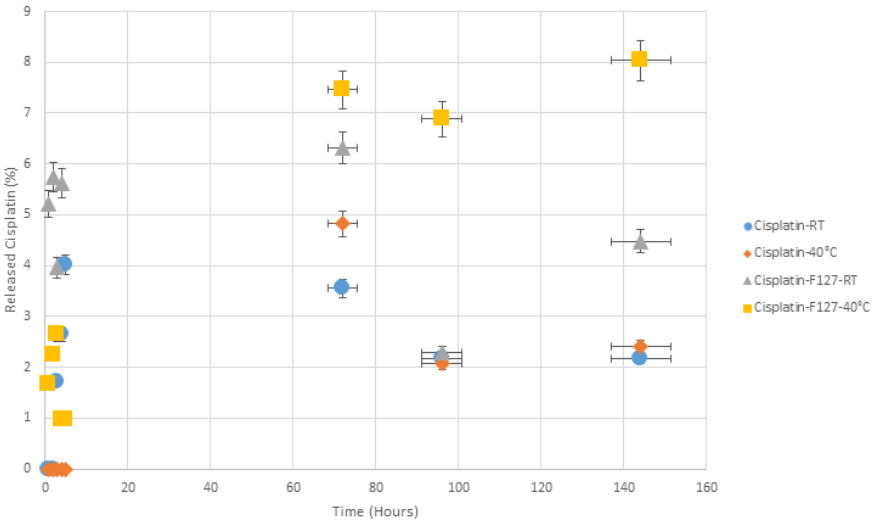

jsd-17-0248-File007.tif

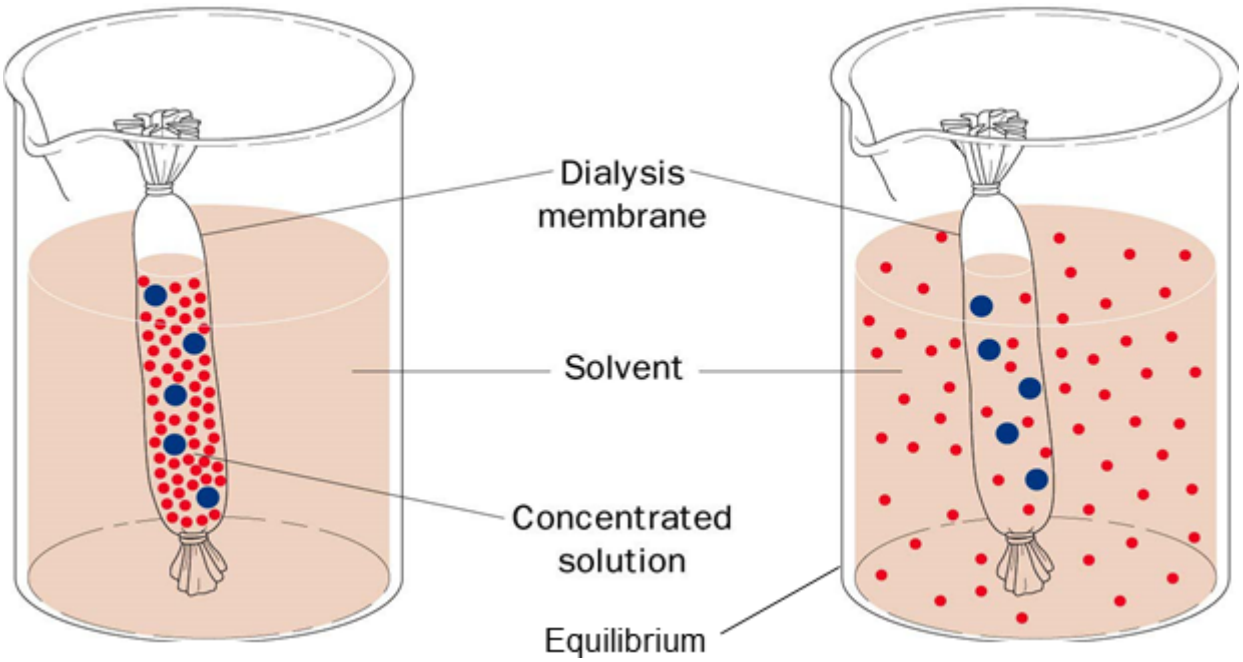

jsd-17-0248-File008.tif

Table 1. Wavelength ranges, concentration ranges, slopes, y-intercepts, and correlation values of malachite green, erythrosin, neat cisplatin, dark colored cisplatin, and cisplatin complex.

Ternary Additive	Wavelength range (nm)	Concentration Ranges (mg/mL)	Slope (Abs/conc.)	Y-intercept (Abs)	R^2
Malachite Green	610-620	0.004 to 0.02	214.5	0.1	0.9897
Erythrosin	520-530	0.008 to 0.04	112.6	0.5	0.9356
Neat Cisplatin	270-300	0.02 to 0.22	0.3	0.008	0.9877
Dark Colored Cisplatin	250-270	0.02 to 0.22	17.1	1.1	0.9011
Cisplatin Complex [47]	700-710 [47]	0.0004 to 0.0014 [47]	0.00022 [47]	8.0×10^{-7} [47]	0.9999 [47]

Table 2. Diffusion coefficient of each experimental condition: neat malachite green, MG, erythrosin, ER, and cisplatin (first 5 hours) and mixed F127 at room temperature, RT, and 40°C. Our results are compared to the in vitro release of cisplatin from core-shell poly(lactide-co-glycolide) (PLGA) nanoparticles [58], PLGA microspheres, solid fibers, and hollow fibers [61], and electrostatically cross-linked chitosan-alginate nanoparticles [62].

Experimental Condition	Diffusion Coefficient (cm^2s^{-1})
MG-RT	$2.6 \pm 0.01 \times 10^{-7}$
MG-F127-RT	$2.6 \pm 0.01 \times 10^{-8}$
MG-40°C	$7.9 \pm 0.1 \times 10^{-7}$
MG-F127-40°C	$5.2 \pm 0.01 \times 10^{-7}$
ER-RT	$4.7 \pm 0.01 \times 10^{-8}$
ER-F127-RT	$3.7 \pm 0.1 \times 10^{-9}$
ER-40°C	$5.2 \pm 0.01 \times 10^{-7}$
ER-F127-40°C	$1.0 \pm 0.01 \times 10^{-6}$
Cisplatin-RT (5 hours)	$6.7 \pm 0.01 \times 10^{-6}$
Cisplatin-F127-RT (5 hours)	$3.0 \pm 0.1 \times 10^{-7}$
Cisplatin-40°C (5 hours)	0
Cisplatin-F127-40°C (5 hours)	$1.2 \pm 0.1 \times 10^{-6}$
Cisplatin-PLGA nanoparticles (150 hours)	4.1×10^{-17} [58]
Cisplatin-PLGA microspheres (500 hours)	4.8×10^{-13} [61]
Cisplatin-PLGA solid fibers (200 hours)	6.1×10^{-10} [61]
Cisplatin-PLGA hollow fibers (400 hours)	3.3×10^{-10} [61]
Cisplatin-chitosan-alginate nanoparticles (t < 2 hours)	8.2×10^{-1} (average) [62]

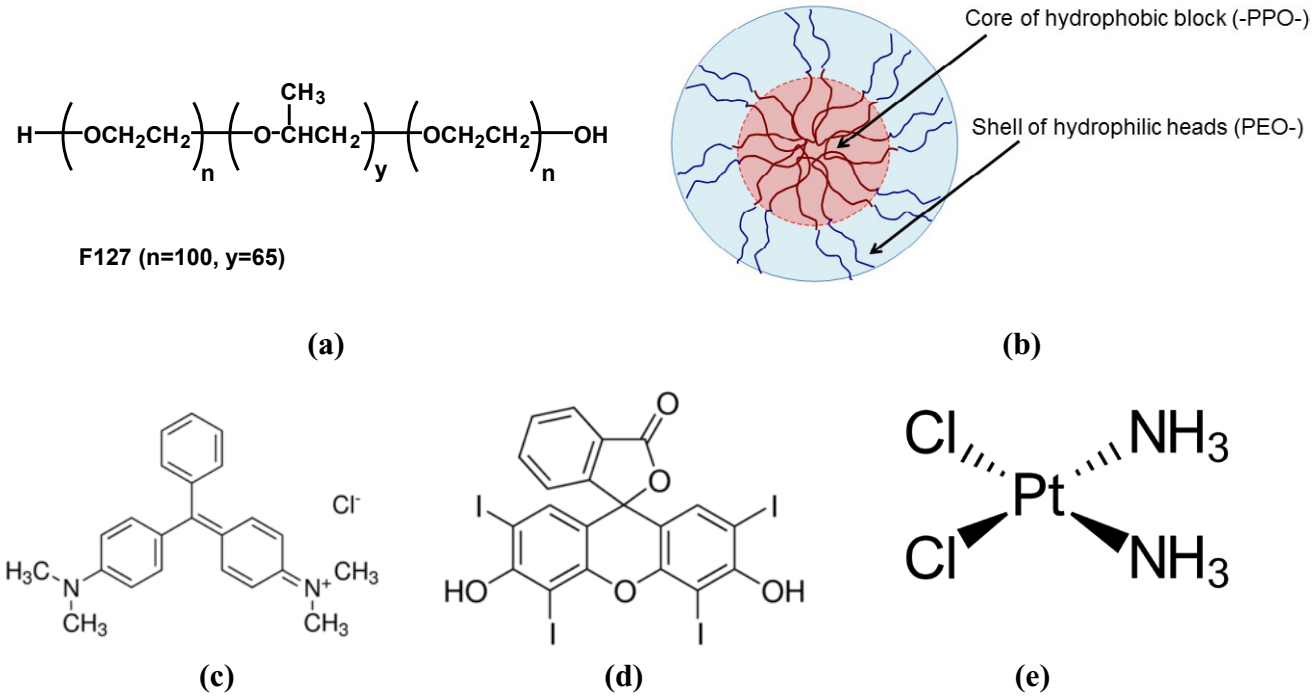

Fig. 1 (a) Pluronic® F127 (b) Example of PEO-PPO-PEO micelle structure (c) Malachite green chloride (d) Erythrosin B dye (e) Cis-dichlorodiammineplatinum(II) (Cisplatin)

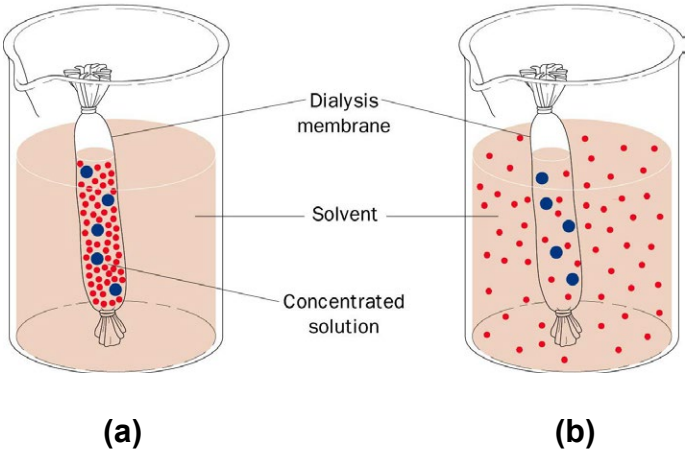

Fig. 2 Setup of dialysis tubing experiment (a) at start of dialysis (b) at equilibrium

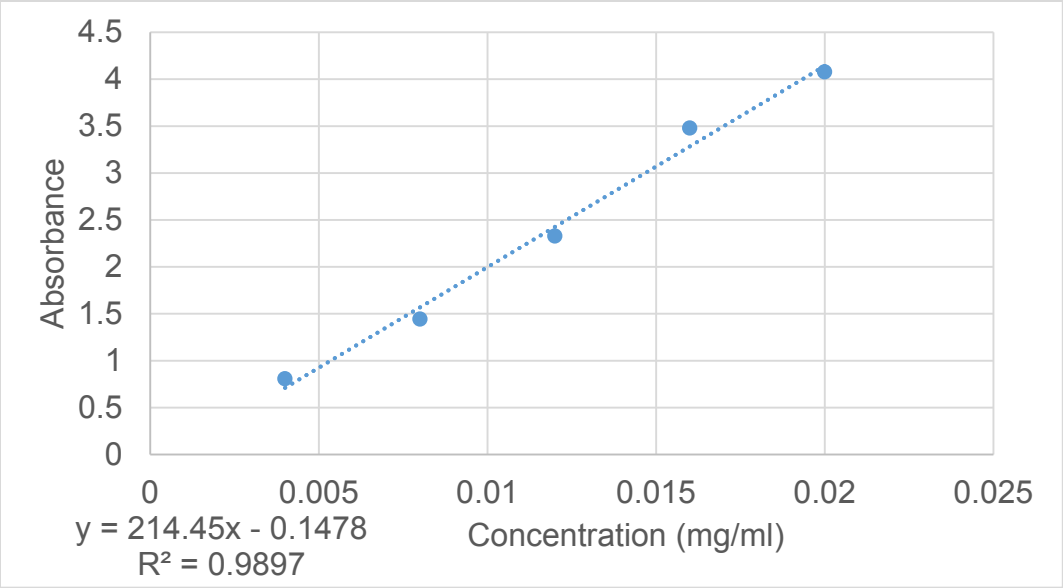

Fig. 3 Neat malachite green absorption vs concentration calibration curve. Absorption analysis were measured in 500ml deionized water using UV-Vis at wavelengths 610-620 nm

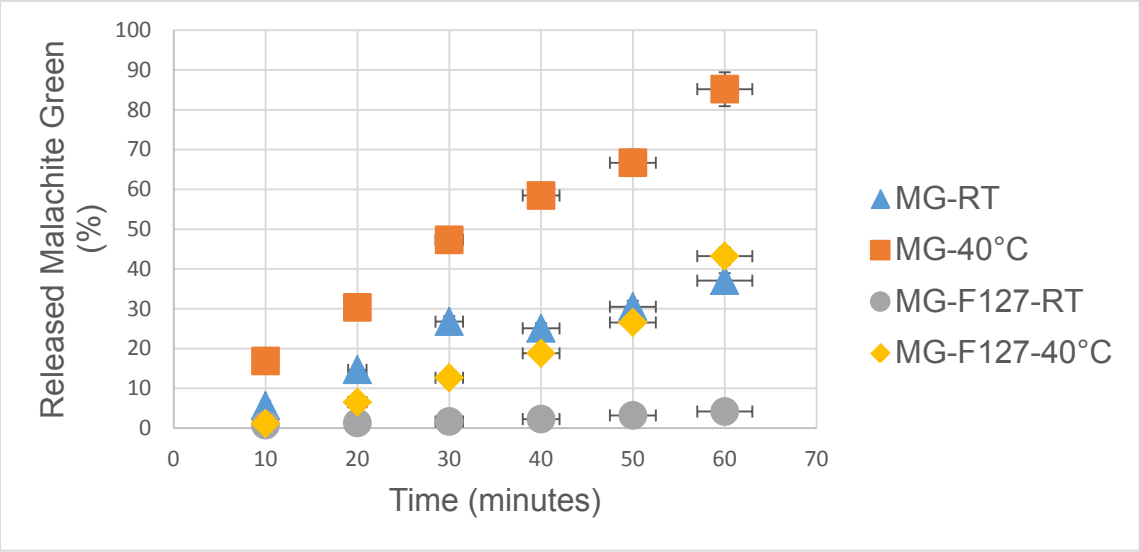

Fig. 4 Release of neat malachite green, MG, and malachite green-F127, MG-F127, at room temperature, RT, and 40°C over time. Each condition the malachite green released was measured in 500ml deionized water by UV-Vis at wavelengths 610-620nm

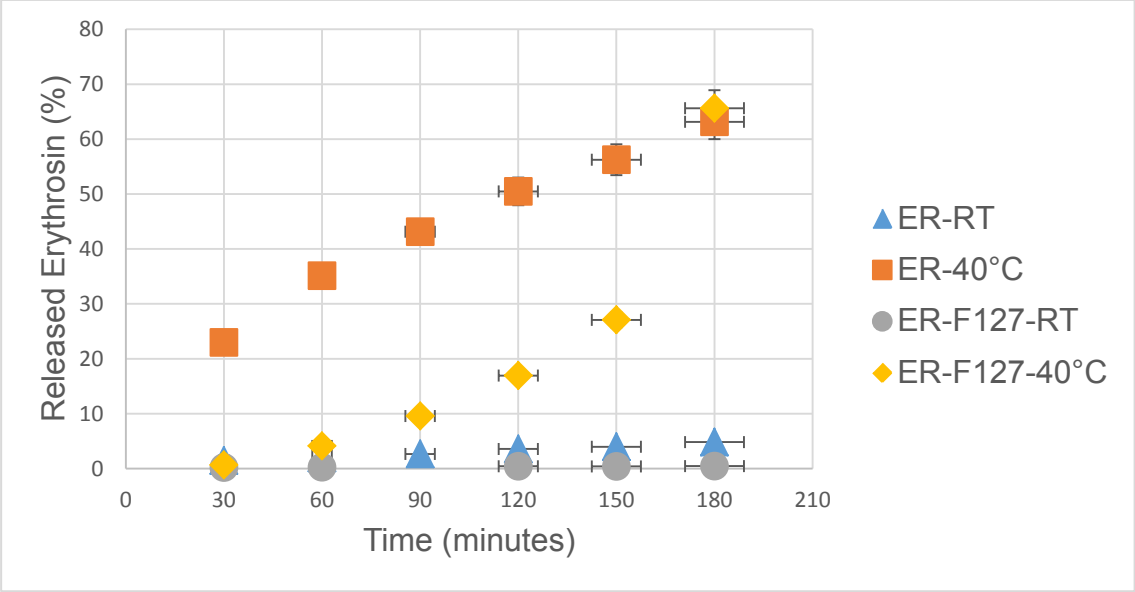

Fig. 5 Release of neat erythrosin, ER, and erythrosin-F127, ER-F127, at room temperature, RT, and 40°C over time. Each condition of the erythrosin released was measured in 500ml deionized water by UV-Vis at wavelengths 520-530nm

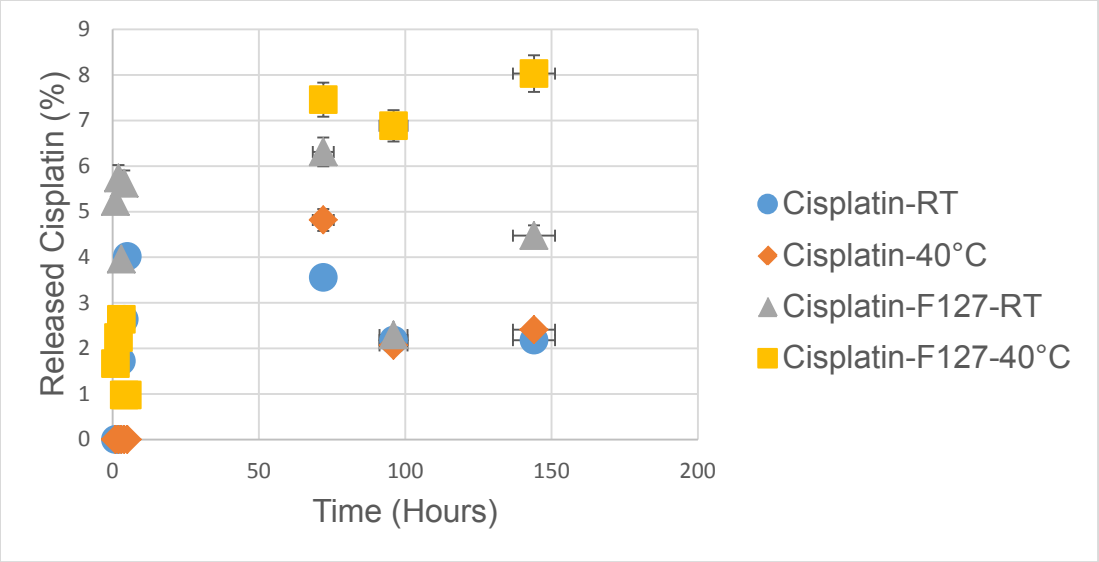

Fig. 6 Release of neat cisplatin and cisplatin-F127 at room temperature, RT, and 40°C over time. Each condition of the cisplatin released was measured in 500ml deionized water by UV-Vis at wavelengths 250-270nm.